Identifying coupled clusters of allostery participants through chemical shift perturbations

Yunyao Xu[a], Dongyu Zhang[a], Rivkah Rogawski[a], Crina M. Nimigean[b,c,d], and Ann E. McDermott[a,1]

[a]Department of Chemistry, Columbia University, New York, NY 10027; [b]Department of Anesthesiology, Weill Cornell Medical College, New York, NY 10065; [c]Department of Biochemistry, Weill Cornell Medical College, New York, NY 10065; and [d]Department of Physiology and Biophysics, Weill Cornell Medical College, New York, NY 10065

Contributed by Ann E. McDermott, December 3, 2018 (sent for review June 28, 2018; reviewed by Vincent J. Hilser, Ayyalusamy Ramamoorthy, and Gianluigi Veglia)

Allosteric couplings underlie many cellular signaling processes and provide an exciting avenue for development of new diagnostics and therapeutics. A general method for identifying important residues in allosteric mechanisms would be very useful, but remains elusive due to the complexity of long-range phenomena. Here, we introduce an NMR method to identify residues involved in allosteric coupling between two ligand-binding sites in a protein, which we call chemical shift detection of allostery participants (CAP). Networks of functional groups responding to each ligand are defined through correlated NMR perturbations. In this process, we also identify allostery participants, groups that respond to both binding events and likely play a role in the coupling between the binding sites. Such residues exhibit multiple functional states with distinct NMR chemical shifts, depending on binding status at both binding sites. Such a strategy was applied to the prototypical ion channel KcsA. We had previously shown that the potassium affinity at the extracellular selectivity filter is strongly dependent on proton binding at the intracellular pH sensor. Here, we analyzed proton and potassium binding networks and identified groups that depend on both proton and potassium binding (allostery participants). These groups are viewed as candidates for transmitting information between functional units. The vital role of one such identified amino acid was validated through site-specific mutagenesis, electrophysiology functional studies, and NMR-detected thermodynamic analysis of allosteric coupling. This strategy for identifying allostery participants is likely to have applications for many other systems.

solid-state NMR | allostery | membrane proteins | ion channel | ligand affinity

Allostery refers to changes in a protein due to perturbations at a remote site, including structural or dynamic alterations (1). Frequently, the change is elicited by binding of a ligand, and is manifested in a consequent change in the affinity of another ligand binding to a different region of the protein. Allostery is a ubiquitous and efficient mechanism for communication in biology. In examples as diverse as enzyme regulation (2), transmembrane cell signaling (3), and gene expression regulation (4), the binding of one ligand to a protein changes the affinity of other ligands binding at distal binding sites, thus controlling "downstream" events.

Many experimental studies have focused on elucidating the molecular mechanism by which the perturbation is propagated within or between the functional units (5, 6), for example, by identifying changes in close contacts between specific residues that are responsible for allostery. Computational methods, such as molecular dynamics simulations, have complemented these experimental strategies by identifying correlated motions of residues, which further clarify the atomistic mechanism by which these residues participate in allostery (6–8). It has been emphasized that there may not be a single set of conformational changes underlying the allostery; rather, ligand binding may shift the protein's conformational and dynamic ensemble, resulting in changes in thermodynamics and affinity at distant sites (9–11). Nevertheless, in many allosteric systems, there are key residues whose participation is important to the underlying mechanism (12). Identifying these key residues, which can be distant from either of the binding sites, is of great interest for a mechanistic understanding of allostery, protein engineering, and drug design.

A number of methods show promise for identifying the key residues involved in allostery. Sequence analysis can identify evolutionary residue pairs as allostery candidates (13). Graph theory can be used to calculate the optimal residue connections for the allosteric network (14). A framework to calculate cooperativity between residues in protein folding was proposed to map the cooperative interaction based on a computationally generated ensemble of partially folded protein (15, 16). A new algorithm called contact networks through alternate conformation transitions uses experimental X-ray data to identify contact networks of conformationally heterogeneous residues (17). Double-mutation cycle methods aim to identify cooperative residue pairs (18, 19). These approaches provide powerful insights; however, identification of allosteric participants can often remain elusive and challenging.

NMR has proven to be a powerful tool to analyze allostery. The study of protein dynamics via NMR provides a unique tool to characterize entropy-driven allostery by dissecting the contribution of dynamics to the coupling energy (9, 20–29). NMR titration studies can quantitatively measure the energetics of the allosteric transition (22, 30, 31). Moreover, analysis of chemical shift perturbations in various states of the protein provides a

Significance

Allostery is a common strategy used by nature to transmit information in proteins, including membrane signaling systems, wherein binding of one ligand affects avidity for binding another ligand in a distal site. Methods are needed for elucidation of functional groups that are critical for coupling between the binding sites, which we call allosteric participants. Identifying and characterizing allosteric participants is important for understanding the allosteric mechanism and crucial for developing new drugs. We develop an NMR method to detect allosteric participants that relies on their multistate nature, and we apply this method to a membrane protein, the potassium channel KcsA. We confirm the importance of specific amino acid side chains for allostery through analysis of binding affinities.

Author contributions: Y.X. and A.E.M. designed research; Y.X. and D.Z. performed research; D.Z. contributed new reagents/analytic tools; Y.X., C.M.N., and A.E.M. analyzed data; and Y.X., D.Z., R.R., C.M.N., and A.E.M. wrote the paper.

Reviewers: V.J.H., Johns Hopkins University; A.R., University of Michigan; and G.V., University of Minnesota.

The authors declare no conflict of interest.

[1]To whom correspondence should be addressed. Email: aem5@columbia.edu.

This article contains supporting information online at www.pnas.org/lookup/suppl/doi:10.1073/pnas.1811168116/-/DCSupplemental.

Published online January 24, 2019.

global snapshot of the various residues affected by a given perturbation, presumably reporting on the allosteric nature of the transition. However, chemical shifts are sensitive to a variety of effects, so methods are needed to dissect those resides whose chemical shift perturbation is specifically due to allosteric coupling. Melacini and coworkers (32) advanced previous chemical shift analysis by introducing chemical shift covariance analysis (CHESCA), which combines singular value decomposition and hierarchical analysis to identify allosterically coupled residues. CHESCA specifically highlights long-range effects of ligand binding that are similar for a large number of ligands. Residues are clustered based on the covariance of chemical shift changes, invoking the assumption that residues belonging to the same functional unit show correlated behavior in terms of NMR shifts.

We demonstrate here a method based on NMR shifts to identify players in allostery for systems with two ligand binding events, which we call chemical shift detection of allostery participants (CAP). Established NMR methods can identify residues directly involved in the binding of a ligand and those that are coupled to the binding of the ligand even if they are distant (33–35), as demonstrated in many prior NMR studies of allostery (9, 36–38). We consider here a system where two separate ligand binding events are allosterically coupled to each other. We hypothesize that in a strongly allosteric protein, a handful of sites are expected to show "multistate" behavior, as manifested in three or more possible chemical shifts, depending on the combination of binding of ligands. Functional groups in the protein can be divided into four groups (Fig. 1*A*): sites that respond to binding of the first ligand, which form a network, including sites distant from the actual ligand binding site (I); analogously, sites that respond to the binding of the second ligand (II); sites that are not sensitive to either ligand binding event (III); and sites that depend on the combination of occupation of the two ligand binding sites (IV). The sites in the last group are expected to be energetically coupled to both binding events, and therefore are strong candidates for involvement in mediating allosteric coupling between the two binding affinities, making them critical to functions. We refer to them as "allostery participants."

We demonstrate this method on the ion channel KcsA reconstituted in 1,2-dioleoylsn-glycero-3-phosphoethanolamine/1,2-dioleoyl-sn-glycero-3-phospho-L-serine(DOPE/DOPS) liposomes (39). KcsA is a 64-kD tetrameric, pH-gated, bacterial potassium channel (Fig. 1 *C* and *D*). KcsA channels, once activated by very low pH, exhibit inactivation, a process where ion channel activity decreases even if the activation stimulus (in this case, exposure to low pH) persists (40–47). Inactivation in KcsA has properties similar to the C-type inactivation described in Shaker channels (41, 48). Inactivation is common in many potassium channels, and it has consequences for channel open times and for refractory periods in action potentials, affecting the channel's control of heartbeat (49).

Many functional and structural studies indicate that an allosteric coupling between the H^+ binding sites (termed the activation gate or pH sensor) and the K^+ binding sites underlies inactivation (41, 44, 46, 47) (Fig. 1*C*). We recently characterized this allosteric system by solid-state NMR and found that protonation of the intracellular pH sensor (which opens the intracellular activation gate) allosterically reduces the K^+ affinity by more than three orders of magnitude at the selectivity filter, which we hypothesized to be the basis for inactivation (30, 50). Previous NMR studies show that the pK_a values of the pH sensor are also dependent on the selectivity filter (44, 47). Crystal structures of KcsA channel constructs with open pH gates also show a correlation between the extent of opening and ion occupancy and structural changes at the selective filter (51, 52). The conformation changes associated with binding or release of K^+ and H^+ are in slow exchange on the NMR time scale (31), meaning that the rate constants are slower than the difference in NMR resonance frequencies (slower than a few milliseconds). This enables us to study all four states of KcsA with respect to ligand binding.

NMR markers of binding of K^+ and H^+ in KcsA were identified in our recent studies (30). The H^+ and K^+ binding units are remote (>30 Å), and the residues involved in the process of transmitting the information between units were not well characterized in our recent studies. KcsA is thus an ideal model to illustrate the CAP method for studying allostery in systems of two coupled remote binding sites. Here, we apply CAP to KcsA in liposome preparations (39) and identify residues that are likely to play a role in allosteric coupling. We subsequently studied the functional effect of mutations in these residues using complementary biophysical methods. Future applications to allosteric transmembrane proteins in native-like environments,

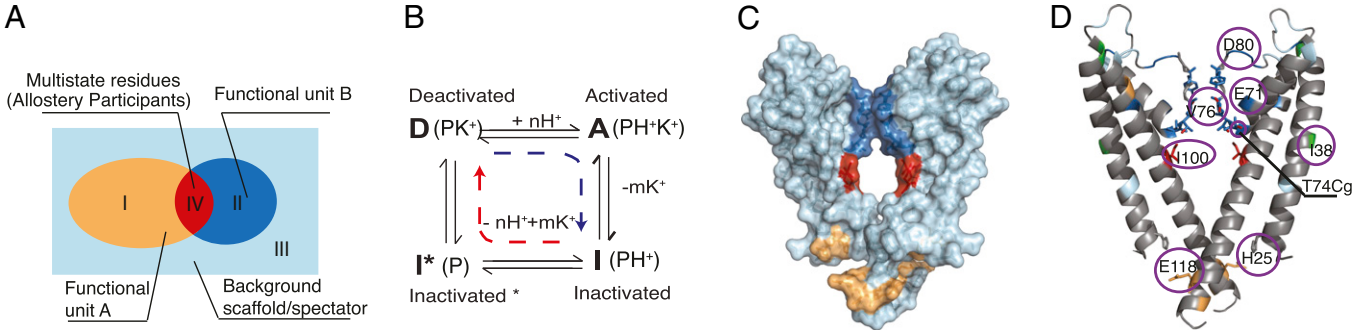

Fig. 1. Residues are clustered into functional units. (*A*) In an allosteric protein with two ligand binding sites, we categorize the residues into the following groups: residues sensitive to binding a single ligand (group I for ligand A and group II for ligand B), spectator residues that are not sensitive to either ligand binding (group III), and residues that are sensitive to both ligands and can report the combination of ligands bound (group IV). CAP analysis is designed to experimentally cluster the NMR preorders for a protein into these four groups. (*B*) Typical four-state allosteric coupling system with two ligands is illustrated using KcsA. P represents the apo protein, and H^+ and K^+ are the ligands. Although the four conditions are strictly defined by their ligand binding status, electrophysiological (functional) terms are suggested for each of the four conditions. The blue dashed line indicates the inactivation process, which has a rate in the range of 10^{-1}–1 s^{-1}; the red dashed line indicates the recovery process, which has a rate in the range of 10^{-1}–10^{-2} s^{-1}. Activation is a transition from D to A, which has a rate in the range of 10^{1}–10^{2} s^{-1} (51). (*C*) Crystal structure (Protein Data Bank ID code 1K4C) of the KcsA potassium channel is color-coded according to the groups outlined in *A*: K^+ binding sites (marine), H^+ binding sites (orange), spectators (light blue), and allostery participants (red), where responses are based on the combination of ligands binding. (*D*) With CAP analysis, we can assign individual residues or sites into groups. The results of CAP analysis are highlighted in the crystal structure of KcsA. Residues belonging to different groups are color-coded as in *C*. Other residues mentioned in the paper are also highlighted in green.

such as G protein-coupled receptors or membrane transporters, are expected to be similarly powerful.

Results

Identifying Residues That Serve as Markers. We began by acquiring NMR spectra of KcsA in four limiting conditions with respect to ligand binding (Fig. 1*B* and *SI Appendix*, Fig. S1). Our goal was to use these spectra to cluster residues into the four groups mentioned above, namely, responsive to K^+ only, responsive to H^+ only, responsive to neither, and responsive to both. For KcsA, the apo state can be achieved with 0.1 μM K^+ at pH 7.5 [referred to as a deeply inactivated state (I*)], the K^+-bound state with 50 mM K^+ at pH 7.5 [referred to as the resting or deactivated state (D)], the H^+-bound state with 0.5 mM K^+ at pH 3.5 [referred to as the inactivated state (I)], and the doubly ligated K^+- and H^+-bound state with 100 mM K^+ at pH 3.5 [referred to as the activated state (A)]. The conditions for preparing these samples were selected based on our previously measured affinity (K_d) values for K^+ at pH 7.5 and pH 3.5 (30, 31). Chemical shift assignments for these samples were made based on a dipolar-assisted rotation resonance (DARR) (53) ^{13}C-^{13}C chemical shift correlation experiment with various mixing times and heteronuclear nitrogen-carbon double–cross-polarization experiments (44) (*Materials and Methods*). Numerous sites in KcsA had chemical shifts that were invariant to ligand concentrations, confirming that the basic fold of the protein is not affected by K^+ or pH over a broad range (*SI Appendix*, Table S1).

KcsA residues that respond to a single ligand are expected to exhibit two chemical shift values in slow exchange, whose peak intensities track the presence or binding of their corresponding ligands. Comparing chemical shifts among this set of spectra in the four sample conditions shows that, indeed, many sites in the protein exhibit two chemical shifts whose intensities depend on a single ligand. Many of these residues are found in the K^+ binding sites or the pH gate, and were used in prior work to study K^+ affinity (30, 31) (*SI Appendix*, Fig. S2). It is notable that residues quite distant from the K^+ and H^+ binding site sometimes exhibit two-state behavior (*SI Appendix*, Fig. 1*D* and Table S1). Some of the remote reporters responding to K^+ binding are located behind the selectivity filter, such as E71 and D80; in the outer mouth of channel, such as Y81 and I60; or in the bilayer-embedded helices, such as I38. Interestingly, these residues do not show a clear physical contact network, but are spread out all over the protein. It is worth noting that atoms within the same residue can have a different chemical shift response to torsion or steric interactions, so they do not always reflect the same trends (54) (*SI Appendix*, Table S1). We discuss details of the assignment of reporters to the two networks more below.

We also observed that a handful of functional groups in key amino acids exhibit more than two chemical shifts, whose intensities reflect the combination of ligand occupancies (Fig. 2*A*). In some cases, a residue's side chain can exhibit three distinct shifts, while the backbone atoms exhibit two. Examples include T74 and T75, in which the CG side chain displays three different chemical shifts (Fig. 2*B*), but the CA and CB side chains only display two chemical shifts each (Fig. 2*A*). We reason that the side-chain atoms have more flexibility, or are in more direct contact with other residues in the networks of both binding pockets. Multistate behavior can manifest as a change in chemical shift, as illustrated by T74 and T75, or as a change in dynamics, as illustrated by the behavior of residue I100 (44) (Fig. 2*B*; 1D slices of I100 peaks are shown in *SI Appendix*, Fig. S3). Allostery has been shown to involve changes in the dynamic behavior of various states as well as in the underlying structure (26, 55). NMR is very sensitive to protein dynamics on time scales from picosecond to seconds (56, 57). For I100, we observed two sets of chemical shifts for the CB-CG2 correlation in the apo, deactivated, and inactivated states; in the activated state (protonated/K^+ binding state), the peak corresponding to I100 is missing, suggesting that it is broadened due to structural inhomogeneity or that its relaxation times are shorter. In either case, it is reasonable to assume that the structure or dynamics of I100 in the activated state are distinct from those in the other states. For these residues (T74, T75, and I100), the populations of the NMR reporters depend on binding of both ligands such that a distinct form is observed if and only if both ligands are simultaneously bound. From this, we conclude that for residues T74, T75, and I100, the local structure and energetics depend on the combination of the binding status of the two ligands (not simply on one ligand or the other). This observation suggests key roles for these residues in allosteric coupling between the two binding sites. Indeed, the role of I100 in mediating the coupling due to its contacts with F103 has been proposed and examined by various methods (58). Also, the importance of the T75 side chain has been identified by showing that T75A mutant lacks inactivation and shows an inverted coupling (59). The side chains of T74 and T75 are similarly located between the proton and potassium ion binding sites, which further supports their potential role in connecting the two networks (Fig. 2*C*). In this work (as discussed below), we also examine the role of T74.

Identifying Networks by Chemical Shift Correlation. The majority of the reporters exhibit two possible NMR peaks over the titration and depend only on one of the ligand binding events. We hypothesized that residues in the same functional unit will experience correlated population changes as ligands are titrated. However, given the strong allosteric coupling, the binding of one ligand will induce binding or release of the other in some regimes, leading to an apparent correlation of the two networks and potential confusion. We clustered the reporters into functional units to identify which ligand each reporter is sensitive to. In other words, for some experimental conditions, a straightforward titration of one variable (e.g., K^+) can lead to changes in binding at the other (H^+) binding site. This complicates separation of the two functional units, as residues that are only affected by one ligand appear to respond to the other ligand. For example, E118 and E120 change chemical shifts between the high- and low-K^+ spectra at neutral pH (44, 47); however, they are known to be the proton binding markers (60). Such correlated binding occurs in a restricted concentration regime. To buttress our assignments of the various reporters distinguishing residues that belong to one reporter network from those in the other network, we include a broad range of conditions, including ones where the binding of the ligands can be separately controlled by concentrations. For example, for KcsA, a K^+ titration done at pH 3.5, where the pH sensor remains protonated throughout the K^+ titration, allowed us to uniquely identify K^+ binding markers. Titrations carried out at pH 7.5 reflect simultaneous changes in both pockets, the direct effects of changing K^+ occupancy in the selectivity filter, and the secondary effects of changing H^+ occupancy in the pH sensor; as expected, both K^+ markers and H^+ markers change.

Titrations were detected using ^{13}C-^{13}C 2D spectra of KcsA, in which the populations for various states can be monitored at a large number of sites by integrating the corresponding peaks since the exchange process is slow [consistent with the millisecond-to-second time scale of the inactivation and recovery process as measured by electrophysiology (51, 61) and the exchange rate estimated by NMR as <500 per second (31)]. The assignments of the residues were verified by other 2D or 3D homo- or heteronuclear correlation. Various residues show different magnitudes of chemical shift change in terms of parts per million (0.5–2 ppm) that are useful in this analysis and are enumerated in *SI Appendix*, Figs. S4 and S5.

As demonstrated by previous NMR studies (32, 62), correlation analysis is a useful tool to evaluate the relationship between two

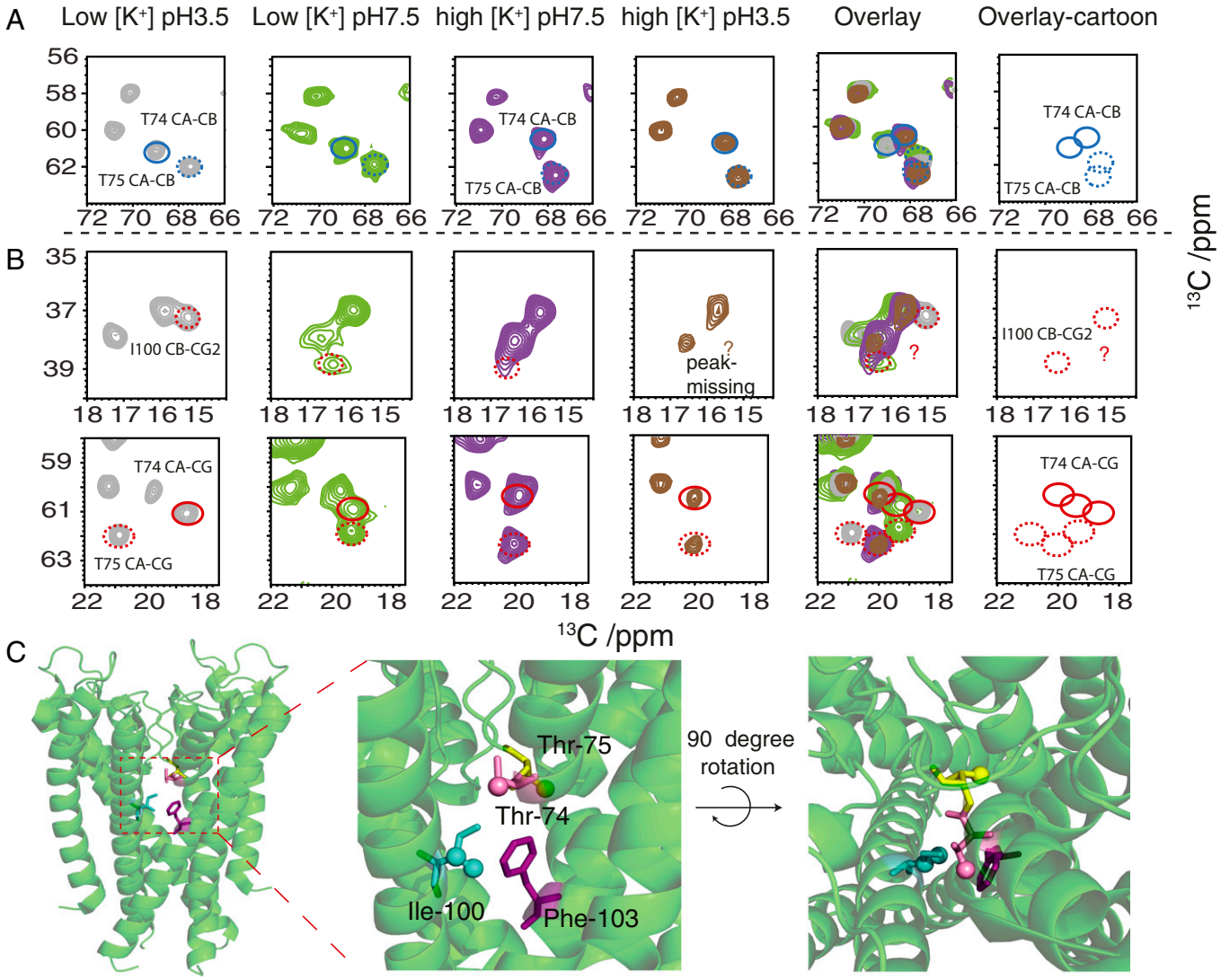

Fig. 2. Two-state and multistate NMR markers are shown on NMR spectra of samples in various K^+, H^+ concentrations. (*A*) Two typical "two-state" NMR markers for K^+ binding are illustrated, namely, T74 (blue circle) and T75 (blue dashed circle) backbone CA and CB correlations. (*B*) Two cases of multistate allostery participants are shown. In the first row, markers I100 CB-CG2 are shown for samples in various conditions and are labeled using a red dashed circle. For samples at low pH and high [K^+], the peak for I100 is not detected. We surmise that this may be due to dynamics or heterogeneous conformations. In any event, the appearance of the peak depends on the combination of ligands present, and not specifically on one or the other ligand. In the second row, two multiple-state markers are shown, the side-chain CG atoms of T74 (red circle) and T75 (red dashed circle), displaying three distinctive chemical shifts for the four spectra of KcsA at various conditions. (*C*) Allosteric participants T74, T75, I100, and F103 are highlighted on a crystal structure (Protein Data Bank ID code 1K4C), indicating plausible connections between the two binding sites on the opposite sides of the membrane in KcsA.

residues. Here, we monitored the population shifts of individual sites as we titrated ligands through the system and then evaluated the Pearson correlation coefficient for residue pairs (as discussed further in *Materials and Methods*):$Conv(X,Y) = E(XY) - E(X)E(Y)/\sqrt{E(X^2) - (E(X))^2}\sqrt{E(Y^2) - (E(Y))^2}$, where X, Y represents an array of population percentage of bound state (peaks dominate in high [K^+] condition) in a series of titration points of the two residues for correlation analysis. From the coefficients, we constructed the covariance matrix of population changes in response to the ligands (Fig. 3 *A*–*D*).

Our results show that the populations of numerous residues are highly correlated throughout the titration: At pH 7.5, we observed a global network, which includes residues in the K^+ binding sites, such as V76, T75, and T74; flanking residues, such as I60, E71, D80, L81, and Y82; and proton binding residues E118/E120 (Fig. 3 *A* and *B*). As mentioned above, near these conditions, a coupled binding event occurs. By contrast, the decoupled transition at pH 3.5 involves only K^+ binding. Many residues exhibit correlated shifts and serve as K^+ binding markers, including residues in the binding site and quite distal residues (Fig. 3*C*). However, the proton binding residue E118 remains protonated throughout the titration at pH 3.5, as is indicated by the flat slope in its correlation with V76 (Fig. 3*D*, *Upper Right*). This flat correlation allows us to filter out this residue as belonging to the proton binding unit, rather than the potassium binding unit, by comparison with the globally coupled network identified at pH 7.5.

We also identified I38 and E51 as residues that show chemical shift changes, but the population changes do not show a strong covariance with other two-state marker sites in response to [K^+] change (Fig. 3 *A* and *C*). E51 is likely a pure proton binding marker, since its chemical shift change is mainly caused by pH change, but not an allosteric marker. For I38, the chemical shift change is more

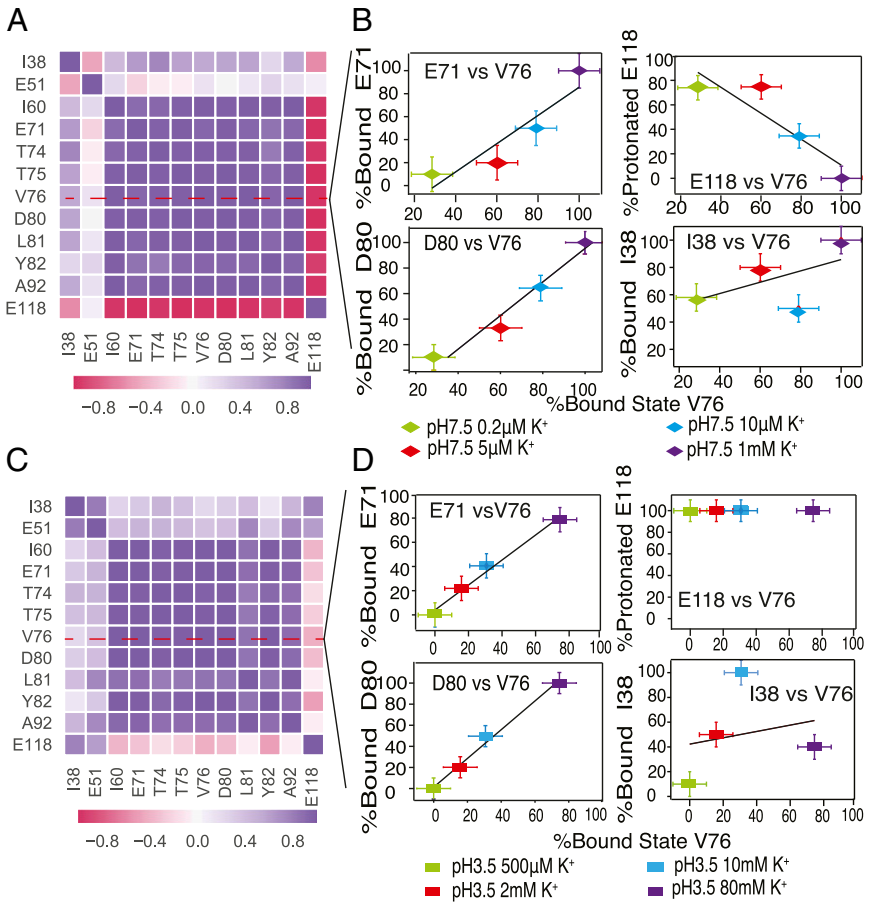

Fig. 3. Chemical shift correlation analysis reveals networks of residues in KcsA involved in binding. Residues that show two alternative forms are analyzed to discern whether they report on K^+ vs. H^+ binding. The covariance of the populations as [K^+] is titrated, as illustrated using a heat map for pH 7.5 (*A*) and pH 3.5 (*C*). To further illustrate, a cross-section at V76 is expanded to show the correlation of V76 populations compared with populations detected for other residues. This analysis was performed at both neutral pH (*B*, diamonds) and acidic pH (*D*, rectangles). A network of potassium binding sites is revealed at pH 3.5 (a condition where potassium binding is decoupled from proton binding in the titration) such that they all report on the same binding event with the same apparent affinity. The network is dispersed throughout the protein and includes I60, E71, T74, T75, V76, D80, L81, Y82, and A92. The correlation network at pH 7.5 also includes E118 because potassium binding at this pH is coupled to proton binding in the titration. E118 shows a negative correlation at neutral pH, since the allosteric coupling causes proton release to be correlated with K^+ binding over a range of solvent conditions. E118 is considered to be a protonation marker for the activation gate. For I38 and E51, we observe very low or no correlation to other residues, such as V76, at both pH values, indicating that the observed chemical shift changes for these residues are likely to be unrelated to binding of these ligands. (Additional correlation plots are shown in *SI Appendix*, Figs. S4 and S5.)

likely to be caused by other environmental factors, which have not been clarified here.

Functional Tests of Putative Allostery Participants. We next studied the allostery participant sites where the chemical shift serves as a marker for the combination of binding states. Such sites exhibit more than two chemical shifts for four distinct combinations of "gates" or binding states. We propose that they are potentially involved in energetic coupling between the two binding sites. We sought corroborative evidence for the role of putative residues identified through their NMR shift behaviors. We examine the functional behavior of site-specific mutations involving the putative coupling participants and compared with WT. I100 and F103 have previously been suggested as possibly important allosteric coupling residues (41, 58) (Fig. 1*C*). Mutagenesis, molecular simulation, and our NMR study have provided strong evidence for the participation of F103 and I100 (30, 41).

T74 is another possible important allostery participant in allosteric coupling, as suggested by this CAP analysis (Fig. 3*A*); it has previously been suspected to interact with F103 and I100 during inactivation (52, 58), but without direct evidence. Its involvement is also difficult to detect simply by comparing crystal structures of various states (*SI Appendix*, Fig. S7). The observation of "multistate behavior" of the NMR peaks for the T74 CG side chain, and its sensitivity to the combination of binding states, led us to propose that the side chain of T74 is important for propagating allostery. To test this hypothesis, we mutated T74 to a serine to remove the CG methyl group of the threonine and characterized the allosteric coupling by NMR, namely, the K^+ affinity changes, as a function of pH. As shown in Fig. 4*A*, the affinity for K^+ in T74S KcsA decreased only fourfold upon switching from pH 5 to pH 3.5 (red), while for WT KcsA, the K^+ affinity decreased 250-fold for the same pH change (purple). Thus, the T74S mutation dramatically reduced the pH sensitivity of the K^+ affinity, indicating that the allosteric coupling network is significantly reduced. This result suggests that channel opening is less coupled to inactivation at the selectivity filter.

To investigate the impact of the T74S mutation on channel activity, we further analyzed this mutant using single-channel recordings in lipid bilayers. As shown in Fig. 4 *B* and *C*, T74S shows long openings and a high open probability. In contrast, WT shows brief openings and a low open probability of 1.4 ± 1.0%

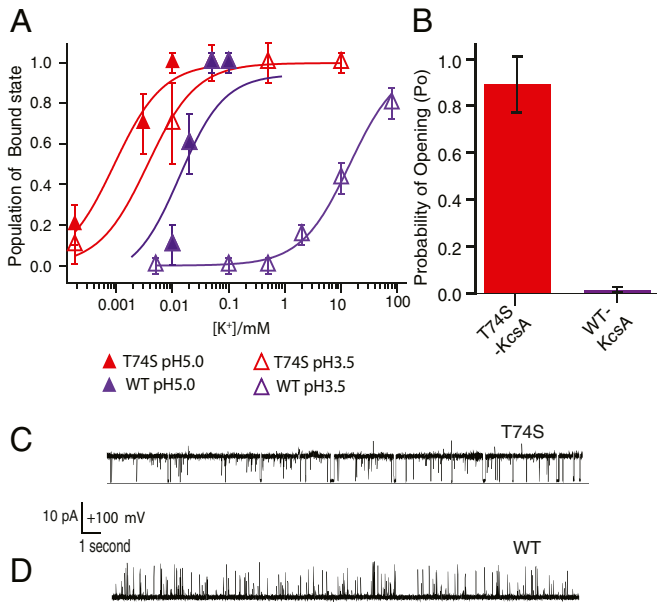

Fig. 4. Mutation of T74S causes a strong reduction of allosteric coupling, indicating that the side chain is a crucial player for propagating allosteric interaction and C-type inactivation. (*A*) NMR-detected titration of T74S with respect to K^+ indicates that the effect of pH on the K^+ affinity (i.e., coupling strength) is much weaker for the T74S mutant compared with WT. A prior titration study on WT shows that the affinity of K^+ is around 250-fold weaker at pH 3.5 than that at pH 5.0. (i.e., 4 mM vs.16 μM, the purple symbols in the plot; taken from ref. 30). Titration of T74S in this study indicates that the affinity for K^+ is only fourfold weaker at pH 3.5 than that at pH 5.0. (i.e., 4 μM vs. 1 μM, the red symbols) The extremely high affinities for K^+ at both pH values suggest that T74S is not only a coupling mutant but also an affinity mutant similar to E71A (42). (*B*) Opening probabilities of T74S and WT-KcsA are 0.89 ± 0.12 and 0.014 ± 0.010, respectively. The values are mean ± SD from nine and three experiments for T74S and WT-KcsA, respectively. The lack of inactivation is consonant with our analysis that this mutant has weak allosteric coupling. (*C* and *D*) Representative single-channel traces for the T74S mutant and WT-KcsA at a voltage of +100 mV. The much higher open probability of T74S than WT is interpreted to mean that the loss of a methyl group has led to failure of inactivation.

(Fig. 4 *B* and *D*). The low open probability of WT is consistent with previous electrophysiological data and is a manifestation of activation-coupled inactivation (51, 63). These results confirm that removing the methyl group of T74 in the T74S mutant leads to partially breaking this communication pathway, and to an essentially "inactivation-less" channel variant. It is remarkable that such a simple chemical change could lead to a large effect in thermodynamics and function.

Discussion and Conclusion

We introduced a method, CAP, for analyzing an allosteric protein with two coupled ligand binding sites. NMR chemical shift analysis was used to cluster the protein into distinct networks of reporters (Fig. 1*A*) and to specifically highlight allostery participants whose conformation depends on the combinations of binding events at the two binding sites. We used ligand concentrations as a perturbation, based on our prior knowledge of the system, to fine-tune our analysis of the clusters. We tested CAP on KcsA, a model pH-gated potassium channel in which potassium and proton binding are allosterically coupled.

We paid specific attention to the residues showing multistate behavior in their chemical shifts, reasoning that these residues could be important allosteric participants. A number of the putative partners in allosteric coupling that resulted from the studies have been confirmed by functional analysis, giving strong support for the power of this kind of analysis. For example, the electrophysiology and NMR characterization of the T74S mutation in KcsA presented here demonstrates the crucial role of the T74 side chain in allosteric coupling, as predicted from the CAP analysis. The critical roles of T75 and I100 in allosteric coupling have also been confirmed by previous electrophysiology and molecular dynamic simulations (58, 59), providing additional examples of the veracity of the predictions from CAP analysis.

The statistical analysis carried out in CAP attempts to distinguish function-related chemical shift perturbations from effects that are not related to function, as illustrated in the cases of I38 and E51 in KcsA. The analysis also clusters the functional groups into networks related to each binding site. For example, E71 in KcsA is located behind the selective filter and is critical for C-type inactivation. One hypothesis is that E71 becomes protonated at low pH, breaks the E71/D80 hydrogen bonding network, and causes inactivation. Alternatively, we show here that E71 is a K^+ binding marker, which is consistent with previous results showing that this residue remains protonated throughout the entire pH range (64).

We propose that CAP analysis may have broader utility for studying allostery in other systems. We provide a tentative experimental workflow for carrying out CAP (*SI Appendix*, Fig. S1). The time scale of the interconversion of protein forms should influence the appearance of the NMR spectra and the details in the approach to identify allosteric participants. In KcsA, the conversion between states is slow in comparison to differences in chemical shifts, so we observed individual peaks for each conformation and calculated their populations. For cases where the various ligand-bound forms are in fast exchange, a single averaged peak would be observed [the chemical shift itself reports on the populations, as demonstrated by Melacini and coworkers (32, 65)], so a hybrid of this method and CHESCA would be more appropriate.

The CAP method, and chemical shift perturbation analysis in general, can be powerfully used to study membrane proteins, as illustrated in this study. Allostery is central to the function of many membrane proteins, and is often difficult to analyze at atomic resolution. Moreover, lipids are important to the function of membrane proteins and are expected to have effects on allosteric coupling in membrane proteins. This was demonstrated for KcsA, for which the potassium affinity shifts by several orders of magnitude between lipid bilayers and detergent solubilized forms (31). This approach may be amenable to many other membrane systems along with other emerging methods, such as strategic isotope labeling or fast magic angle spinning, both of which have been applied on the outer membrane protein G from *E. Coli* (66).

CAP can be compared with a number of other methods for analyzing allosteric couplings. For example, in CHESCA, residues can be clustered into groups for ligand binding and allostery based on their chemical shift change (essentially population change) in response to a library of agonists and antagonists (27, 32). A similar analysis was obtained for a barrel enzyme by introducing Ala-to-Gly mutations at various sites and clustering the results based on responses to the mutations (67). In another study of an allosteric system, mutations were specifically introduced at the catalytic site, causing chemical shift change at the hidden allosteric sites due to the reciprocal interactions between an allosteric site and its coupled orthosteric site (68). We add to these prior analyses the emphasis on correlated or joint responses to two different binding sites, and the multiple environments that result, which connect NMR analysis to one of the essential energetic and functional features of allostery. We expect that multiple NMR lines from allostery participants will likely be observed in many other systems. One recent example has been observed in the GTPase atlastin: Residue F151 displays multiple conformation states in the crystal structures collected in various states and is reasoned to be the connecting residue between the active and nucleotide binding sites (69). Such a "multiple-states" behavior

takes advantage of the inherent plasticity of proteins in their response to multiple external stressors. Clearly, not every allosteric participant will be detected in an analysis like CAP, but we propose that this analysis could produce a useful set of hypotheses for functional testing.

Although allostery and activation-coupled inactivation in KcsA have been studied in the past, CAP analysis allowed us to obtain a better understanding of the molecular underpinnings of the coupling (Fig. 1*D*) and the roles of specific residues. Remarkably, we observed a high overlap between the residues identified as energetically or structurally connected to both binding events and those residues whose mutants show functional changes in allosteric coupling strength, demonstrating the power of CAP analysis as a tool for detecting allosteric participants.

Materials and Methods

Protein Sample Preparation. KcsA protein expression and purification protocols and reconstitution into bilayers (DOPE/DOPS = 9:1) for NMR are as described in a previous study (30). To adjust pH and $[K^+]$, the proteoliposomes were first dialyzed against pH 7.5 buffer with appropriate $[K^+]$ (two to three changes), and then further dialyzed at 4 °C against 10 mM sodium citrate buffer at pH 3.5 with the appropriate $[K^+]$ until the pH reached equilibrium (typically 5 h). The pH of the supernatant was confirmed to be within 0.1 unit of the desired value. For all dialysis buffers, the total ion concentration ($[K^+] + [Na^+]$) was maintained at 50 mM, with the exception of the 80 mM $[K^+]$ sample at pH 3.5. The samples were centrifuged to form hydrated pellets and packed in 3.2-mm Bruker rotors for NMR experiments after three rounds of freeze/thaw cycles to remove extra buffer solution.

The plasmid for the T74S mutant was made using gene synthesis, and its sequence was verified by Genewiz. On Coomassie-stained SDS gels, the mutant shows a similar band with WT-KcsA around 70 kDa (*SI Appendix*, Fig. S6), which indicates that the mutant maintains the characteristic tetrameric structure.

NMR Experiments. Approximately 10-mg ^{13}C-^{15}N KcsA samples were used for each NMR experiment. NMR spectra were collected on a Bruker 750-MHz or 600-MHz spectrometer, and spinning rates of 12 kHz or 14 kHz were applied to avoid side-band overlap with regions of interest. For protein assignment, DARR with various mixing times (15 ms, 50 ms, 100 ms, and 200 ms) and NCOCX (N-C′-$C_{i-1,sidechain}$), NCACX (N-Cα-$C_{i,sidechain}$), and DREAM (dipolar recoupling enhanced by amplitude modulation) (70) were applied. For titration curves, DARR (15-ms mixing time) was used, with a calibrated sample temperature at 0 ± 2 °C.

Typical 90-pulse lengths are ∼2.5 μs for proton, ∼5 μs for carbon, and ∼8 μs for nitrogen. We employed 95- to 100-kHz decoupling using two-pulse phase-modulated (TPPM) (71) in proton channels during acquisition. Carbon chemical shifts were referenced externally to the downfield adamantane line at 40.48 ppm, and nitrogen chemical shifts are referenced accordingly by calculation. The spectra were processed in NMRPipe with −30-Hz Lorentzian and 90-Hz Gaussian apodization. Sparky (72) was used for spectral visualization and integration of cross-peaks.

Electrophysiology. T74S and WT KcsA purified protein was reconstituted into liposomes [3:1 1-palmitoyl-2-oleoyl-sn-glycero-3-phosphoethanolamine/1-palmitoyl-2-oleoyl-sn-glycero-3-phospho-(1′-rac-glycerol) (POPE/POPG)] at a concentration of 1 μg/mg of lipid, and stored at −80 °C. Liposomes, thawed on the day of use and sonicated briefly, were applied to artificial lipid bilayers made of 3:1 POPE/POPG dissolved in decane at a concentration of 10 mg/mL. The lipid bilayers are formed over a 100-μm-diameter hole in a transparency partition separating two aqueous chambers in a horizontal lipid bilayer setup, as described by Posson et al. (60). The *trans* recording chamber contained a buffer solution with 10 mM succinate (pH 4.0) and 100 mM KCl, and the *cis* chamber (where liposomes are applied) contained a buffer solution with 10 mM Hepes (pH 7.0) and 100 mM KCl. Current traces were recorded under voltage clamp at +100 mV with an Axopatch 200B amplifier (Molecular Devices), sampled at 20 kHz. The data were further filtered offline at 2 kHz, processed, and analyzed using Clampex and Clampfit v10 (Molecular Devices).

Single-channel current amplitudes were measured by hand from recordings lasting longer than 15 s, and NPo (N, number of channels; Po, open probability of a single channel) values were determined from nine traces for T74S mutant and three traces for WT-KcsA with the Single-Channel Search module from Clampfit. Single-channel open probabilities for T74S mutant were then determined by dividing the NPo by the total number of channels. For WT-KcsA, due to the low opening probability, the total number of channels is difficult to determine; therefore, only the NPo is reported in this paper.

Data Processing. The normalized population ratios were used for K^+ affinity measurement and correlation analysis. The K_d values were measured in Igor Pro (WaveMetrics) by fitting to the titration curve using the following equation: $\theta = [K^+]^n/([K^+]^n + K_d$, where θ is the normalized bound-state population ratio and the Hill coefficient n is fixed to be 1. Pearson correlations analysis was calculated in Mathematica (Wolfram). The values are used to plot the heat map covariance plot in Fig. 3. The linear fitting is done in Igor Pro. The error reported in the paper mainly comes from the fitting, as well as the population integration and averaging between several marker peaks. The crystal structures presented in the paper were prepared with Pymol (Schrodinger).

ACKNOWLEDGMENTS. We thank Dr. Keith Fritzsching for helpful discussion. We thank Dr. Philipp Schmidpeter in the laboratory of C.M.N. for help on electrophysiology measurement. We thank Dr. Mike Goger and Dr. Boris Itin at the New York Structural Biology Center (NYSBC) for support with NMR instrumentation. A.E.M. is a member of the NYSBC. The NMR data were collected at the NYSBC with support from the Center on Macromolecular Dynamics by NMR Spectroscopy, a Biomedical Technology Research Resource supported by the NIH through Grant P41 GM118302. The NYSBC is also enabled by a grant from the Empire State Division of Science Technology and Innovation and by Office of Research Infrastructure Programs/NIH Facility Improvement Grant CO6RR015495. This work was supported by NIH Grant R01 GM088724 (to A.E.M). This work was supported, in part, by NIH Grant R01 GM088352 (to C.M.N.).

1. Cui Q, Karplus M (2008) Allostery and cooperativity revisited. *Protein Sci* 17: 1295–1307.
2. Dokholyan NV (2016) Controlling allosteric networks in proteins. *Chem Rev* 116: 6463–6487.
3. Changeux J-P, Edelstein SJ (2005) Allosteric mechanisms of signal transduction. *Science* 308:1424–1428.
4. Maniatis T, Reed R (2002) An extensive network of coupling among gene expression machines. *Nature* 416:499–506.
5. Sadovsky E, Yifrach O (2007) Principles underlying energetic coupling along an allosteric communication trajectory of a voltage-activated K+ channel. *Proc Natl Acad Sci USA* 104:19813–19818.
6. Feher VA, Durrant JD, Van Wart AT, Amaro RE (2014) Computational approaches to mapping allosteric pathways. *Curr Opin Struct Biol* 25:98–103.
7. Vesper MD, de Groot BL (2013) Collective dynamics underlying allosteric transitions in hemoglobin. *PLoS Comput Biol* 9:e1003232.
8. Rodgers TL, et al. (2013) Modulation of global low-frequency motions underlies allosteric regulation: Demonstration in CRP/FNR family transcription factors. *PLoS Biol* 11:e1001651.
9. Petit CM, Zhang J, Sapienza PJ, Fuentes EJ, Lee AL (2009) Hidden dynamic allostery in a PDZ domain. *Proc Natl Acad Sci USA* 106:18249–18254.
10. Popovych N, Sun S, Ebright RH, Kalodimos CG (2006) Dynamically driven protein allostery. *Nat Struct Mol Biol* 13:831–838.
11. Motlagh HN, Wrabl JO, Li J, Hilser VJ (2014) The ensemble nature of allostery. *Nature* 508:331–339.
12. Nussinov R, Tsai C-JJ (2013) Allostery in disease and in drug discovery. *Cell* 153: 293–305.
13. Lockless SW, Ranganathan R (1999) Evolutionarily conserved pathways of energetic connectivity in protein families. *Science* 286:295–299.
14. Vendruscolo M, Dokholyan NV, Paci E, Karplus M (2002) Small-world view of the amino acids that play a key role in protein folding. *Phys Rev E Stat Nonlin Soft Matter Phys* 65:061910.
15. Pan H, Lee JC, Hilser VJ (2000) Binding sites in Escherichia coli dihydrofolate reductase communicate by modulating the conformational ensemble. *Proc Natl Acad Sci USA* 97:12020–12025.
16. Hilser VJ, Dowdy D, Oas TG, Freire E (1998) The structural distribution of cooperative interactions in proteins: Analysis of the native state ensemble. *Proc Natl Acad Sci USA* 95:9903–9908.
17. van den Bedem H, Bhabha G, Yang K, Wright PE, Fraser JS (2013) Automated identification of functional dynamic contact networks from X-ray crystallography. *Nat Methods* 10:896–902.
18. Schreiber G, Fersht AR (1995) Energetics of protein-protein interactions: Analysis of the barnase-barstar interface by single mutations and double mutant cycles. *J Mol Biol* 248:478–486.
19. Gleitsman KR, Shanata JAP, Frazier SJ, Lester HA, Dougherty DA (2009) Long-range coupling in an allosteric receptor revealed by mutant cycle analysis. *Biophys J* 96: 3168–3178.
20. Sugase K, Dyson HJ, Wright PE (2007) Mechanism of coupled folding and binding of an intrinsically disordered protein. *Nature* 447:1021–1025.

21. Ahuja LG, et al. Mutation of a kinase allosteric node uncouples dynamics linked to phosphotransfer. *Proc Natl Acad Sci USA* 114:E931–E940.
22. Lisi GP, Loria JP (2016) Solution NMR spectroscopy for the study of enzyme allostery. *Chem Rev* 116:6323–6369.
23. Baldwin AJ, Kay LE (2009) NMR spectroscopy brings invisible protein states into focus. *Nat Chem Biol* 5:808–814.
24. Velyvis A, Yang YR, Schachman HK, Kay LE (2007) A solution NMR study showing that active site ligands and nucleotides directly perturb the allosteric equilibrium in aspartate transcarbamoylase. *Proc Natl Acad Sci USA* 104:8815–8820.
25. Zhuravleva A, Gierasch LM (2015) Substrate-binding domain conformational dynamics mediate Hsp70 allostery. *Proc Natl Acad Sci USA* 112:E2865–E2873.
26. Boulton S, Melacini G (2016) Advances in NMR methods to map allosteric sites: From models to translation. *Chem Rev* 116:6267–6304.
27. Akimoto M, et al. (2013) Signaling through dynamic linkers as revealed by PKA. *Proc Natl Acad Sci USA* 110:14231–14236.
28. Swain JF, et al. (2007) Hsp70 chaperone ligands control domain association via an allosteric mechanism mediated by the interdomain linker. *Mol Cell* 26:27–39.
29. Tzeng S-R, Kalodimos CG (2012) Protein activity regulation by conformational entropy. *Nature* 488:236–240.
30. Xu Y, Bhate MP, McDermott AE (2017) Transmembrane allosteric energetics characterization for strong coupling between proton and potassium ion binding in the KcsA channel. *Proc Natl Acad Sci USA* 114:8788–8793.
31. Bhate MP, Wylie BJ, Tian L, McDermott AE (2010) Conformational dynamics in the selectivity filter of KcsA in response to potassium ion concentration. *J Mol Biol* 401: 155–166.
32. Selvaratnam R, Chowdhury S, VanSchouwen B, Melacini G (2011) Mapping allostery through the covariance analysis of NMR chemical shifts. *Proc Natl Acad Sci USA* 108: 6133–6138.
33. Williamson MP (2013) Using chemical shift perturbation to characterise ligand binding. *Prog Nucl Magn Reson Spectrosc* 73:1–16.
34. Hajduk PJ, Meadows RP, Fesik SW (1997) Discovering high-affinity ligands for proteins. *Science* 278:497–499.
35. Mayer M, Meyer B (1999) Characterization of ligand binding by saturation transfer difference NMR spectroscopy. *Angew Chem Int Ed Engl* 38:1784–1788.
36. Whittier SK, Hengge AC, Loria JP (2013) Conformational motions regulate phosphoryl transfer in related protein tyrosine phosphatases. *Science* 341:899–903.
37. Liu JJ, Horst R, Katritch V, Stevens RC, Wüthrich K (2012) Biased signaling pathways in β2-adrenergic receptor characterized by 19F-NMR. *Science* 335:1106–1110.
38. Xu J, et al. (2008) Bicelle-enabled structural studies on a membrane-associated cytochrome B_5 by solid-state MAS NMR spectroscopy. *Angew Chem Int Ed Engl* 47: 7864–7867.
39. Bhate MP, et al. (2013) Preparation of uniformly isotope labeled KcsA for solid state NMR: Expression, purification, reconstitution into liposomes and functional assay. *Protein Expr Purif* 91:119–124.
40. Hoshi T, Armstrong CM (2013) C-type inactivation of voltage-gated K+ channels: Pore constriction or dilation? *J Gen Physiol* 141:151–160.
41. Cuello LG, Jogini V, Cortes DM, Perozo E (2010) Structural mechanism of C-type inactivation in K(+) channels. *Nature* 466:203–208.
42. Cordero-Morales JF, et al. (2007) Molecular driving forces determining potassium channel slow inactivation. *Nat Struct Mol Biol* 14:1062–1069.
43. Devaraneni PK, et al. (2013) Semisynthetic K+ channels show that the constricted conformation of the selectivity filter is not the C-type inactivated state. *Proc Natl Acad Sci USA* 110:15698–15703.
44. Wylie BJ, Bhate MP, McDermott AE (2014) Transmembrane allosteric coupling of the gates in a potassium channel. *Proc Natl Acad Sci USA* 111:185–190.
45. Li J, et al. (2017) Chemical substitutions in the selectivity filter of potassium channels do not rule out constricted-like conformations for C-type inactivation. *Proc Natl Acad Sci USA* 114:11145–11150.
46. Imai S, Osawa M, Takeuchi K, Shimada I (2010) Structural basis underlying the dual gate properties of KcsA. *Proc Natl Acad Sci USA* 107:6216–6221.
47. Ader C, et al. (2009) Coupling of activation and inactivation gate in a K+-channel: Potassium and ligand sensitivity. *EMBO J* 28:2825–2834.
48. Choe S (2002) Potassium channel structures. *Nat Rev Neurosci* 3:115–121.
49. Curran ME, et al. (1995) A molecular basis for cardiac arrhythmia: HERG mutations cause long QT syndrome. *Cell* 80:795–803.
50. Thomson AS, et al. (2014) Initial steps of inactivation at the K+ channel selectivity filter. *Proc Natl Acad Sci USA* 111:E1713–E1722.
51. Chakrapani S, Cordero-Morales JF, Perozo E (2007) A quantitative description of KcsA gating I: Macroscopic currents. *J Gen Physiol* 130:465–478.
52. Cuello LG, et al. (2010) Structural basis for the coupling between activation and inactivation gates in K(+) channels. *Nature* 466:272–275.
53. Takegoshi K, Nakamura S, Terao T (2001) 13C–1H dipolar-assisted rotational resonance in magic-angle spinning NMR. *Chem Phys Lett* 344:631–637.
54. Case DA (1998) The use of chemical shifts and their anisotropies in biomolecular structure determination. *Curr Opin Struct Biol* 8:624–630.
55. Manley G, Loria JP (2012) NMR insights into protein allostery. *Arch Biochem Biophys* 519:223–231.
56. McDermott AE (2004) Structural and dynamic studies of proteins by solid-state NMR spectroscopy: Rapid movement forward. *Curr Opin Struct Biol* 14:554–561.
57. Akke M, Brueschweiler R, Palmer AG (1993) NMR order parameters and free energy: An analytical approach and its application to cooperative calcium(2+) binding by calbindin D9k. *J Am Chem Soc* 115:9832–9833.
58. Pan AC, Cuello LG, Perozo E, Roux B (2011) Thermodynamic coupling between activation and inactivation gating in potassium channels revealed by free energy molecular dynamics simulations. *J Gen Physiol* 138:571–580.
59. Labro AJ, Cortes DM, Tilegenova C, Cuello LG (2018) Inverted allosteric coupling between activation and inactivation gates in K^+ channels. *Proc Natl Acad Sci USA* 115: 5426–5431.
60. Posson DJ, Thompson AN, McCoy JG, Nimigean CM (2013) Molecular interactions involved in proton-dependent gating in KcsA potassium channels. *J Gen Physiol* 142: 613–624.
61. Chakrapani S, Cordero-Morales JF, Perozo E (2007) A quantitative description of KcsA gating II: Single-channel currents. *J Gen Physiol* 130:479–496.
62. Masterson LR, Mascioni A, Traaseth NJ, Taylor SS, Veglia G (2008) Allosteric cooperativity in protein kinase A. *Proc Natl Acad Sci USA* 105:506–511.
63. Gao L, Mi X, Paajanen V, Wang K, Fan Z (2005) Activation-coupled inactivation in the bacterial potassium channel KcsA. *Proc Natl Acad Sci USA* 102:17630–17635.
64. Bhate MP, McDermott AE (2012) Protonation state of E71 in KcsA and its role for channel collapse and inactivation. *Proc Natl Acad Sci USA* 109:15265–15270.
65. Boulton S, Akimoto M, Selvaratnam R, Bashiri A, Melacini G (2014) A tool set to map allosteric networks through the NMR chemical shift covariance analysis. *Sci Rep* 4: 7306.
66. Retel JS, et al. (2017) Structure of outer membrane protein G in lipid bilayers. *Nat Commun* 8:2073.
67. Axe JM, et al. (2014) Amino acid networks in a $(\beta/\alpha)_8$ barrel enzyme change during catalytic turnover. *J Am Chem Soc* 136:6818–6821.
68. Cui DS, Beaumont V, Ginther PS, Lipchock JM, Loria JP (2017) Leveraging reciprocity to identify and characterize unknown allosteric sites in protein tyrosine phosphatases. *J Mol Biol* 429:2360–2372.
69. O'Donnell JP, Byrnes LJ, Cooley RB, Sondermann H (2018) A hereditary spastic paraplegia-associated atlastin variant exhibits defective allosteric coupling in the catalytic core. *J Biol Chem* 293:687–700.
70. Verel R, Ernst M, Meier BH (2001) Adiabatic dipolar recoupling in solid-state NMR: The DREAM scheme. *J Magn Reson* 150:81–99.
71. Bennett AE, Rienstra CM, Auger M, Lakshmi KV, Griffin RG (1995) Heteronuclear decoupling in rotating solids. *J Chem Phys* 103:6951–6958.
72. Goddard TD, Kneller DG (2008) Sparky 3 (University of California, San Francisco).